
A COMPREHENSIVE NUMERICAL INVESTIGATION OF A COUPLED MATHEMATICAL MODEL OF NEURONAL EXCITABILITY

A PREPRINT

 **Burcu Gürbüz***

Institute of Mathematics
Johannes Gutenberg-University Mainz
55128 Mainz, Germany

Institute for Quantitative and Computational Biosciences (IQCB)
Johannes Gutenberg-University Mainz
55128 Mainz, Germany
burcu.gurbuz@uni-mainz.de

 **Aytül Gökçe**

Department of Mathematics
Ordu University
52200 Ordu, Turkey
aytulgokce@odu.edu.tr

 **Mahmut Modanlı**

Department of Mathematics
Harran University
63300 Şanlıurfa, Turkey
mmodanli@harran.edu.tr

January 31, 2025

ABSTRACT

Being an example for a relaxation oscillator, the FitzHugh–Nagumo model has been widely employed for describing the generation of action potentials. In this paper, we begin with a biological interpretation of what the subsequent mathematical and numerical analyses of the model entail. The interaction between action potential variable and recovery variable is then revisited through linear stability analysis around the equilibrium and local stability conditions are determined. Analytical results are compared with numerical simulations. The study aims to show an alternative approach regarding Taylor polynomials and constructed difference scheme which play a key role in the numerical approach for the problem. The robustness of the schemes is investigated in terms of convergence and stability of the techniques. This systematic approach by the combination of numerical techniques provides beneficial results which are uniquely designed for the FitzHugh–Nagumo model. We describe the matrix representations with the collocation points. Then the method is applied in order to acquire a system of nonlinear algebraic equations. On the other hand, we apply finite difference scheme and its stability is also performed. Moreover, the numerical simulations are shown. Consequently, a comprehensive investigation of the related model is examined.

Keywords FitzHugh–Nagumo model · Taylor collocation method · Stability analysis · Dynamical system · Finite difference scheme

1 Introduction

Tracing back its roots to seminal works by Richard FitzHugh in 1961 FitzHugh [1961] and Jin-Ichi Nagumo in 1962 Nagumo et al. [1962], the FitzHugh–Nagumo model (FHN) is often considered to model excitable systems and represents a two component simplified version of well known Hodgkin–Huxley model (HH) Rocsoreanu et al. [2012], Tuckwell and Rodriguez [1998], Jones [1984], Sato and Doi [1992]. This transition to two variable

*Corresponding author

model developed by FitzHugh was made possible through The van der Pol equations to understand nonlinear relaxation oscillators FitzHugh [1961], Izhikevich and FitzHugh [2006]. Here, a further analysis of this model with the addition of several terms inspired FitzHugh to expand this knowledge with a simplified adaptation of the Bonhoeffer van der Pol model (BVP), that has been renowned as FitzHugh–Nagumo model FitzHugh [1961], Izhikevich and FitzHugh [2006]. Although the development of biophysically more realistic HH model was a breakthrough to understand how action potentials arise and propagate, two variable FHN model provided simple and conceptual approach that would not only capture the fundamental aspects surrounding neuronal excitability, but also allow for phase plane methods to gain a better understanding of spike generation Tuckwell and Rodriguez [1998], Sherwood et al. [2014], Faghieh et al. [2010], Kostova et al. [2004].

Although the FHN model is originally use to understand the action potential of single neurons, it has been broadly exploited for many reaction diffusion systems whose components comprise a fast activator variable and a slow inhibitor variable. Thus, the model can be amenable to deal with various dynamics in excitable media and still described as a corner stone for models that exhibit similar characteristics Onyejekwe [2021], Izhikevich et al. [2003]. In addition to capturing neural spiking behaviours, this model has been adapted to describe a wide spectrum of excitable media from the Belousov-Zhabotinsky chemical reaction Pertsov et al. [1984] to slime mold amoeba Vasiev et al. [1994] to cardiac tissue Aliev and Panfilov [1996], Glass and Josephson [1995], Panfilov and Keener [1995].

The generic FHN model is driven by two variables of state, representing both membrane potential and refractoriness (or recovery). Equipped with the FHN model, we investigate its stability by considering a small perturbation around the equilibrium point and its corresponding Taylor expansion. By expressing the linearised system in vector form with the Jacobian matrix evaluated at this point, we seek exponential solutions; this leads to the characteristic polynomial. This approach is followed by many researchers to gain better insights about solution states of real life problems, see for example Murray [2001], Liao et al. [2007], Seydel [2009] for a comprehensive overview. Due to the complexity of the characteristic equation, we firstly consider that no input current is applied. Once this is achieved, we derive conditions needed for various dynamical characteristics and explore the model in more depth for which we conduct bifurcation analysis when non-zero current is applied. We expand upon this extensive body of knowledge by refining the FHN model further.

The numerical investigation of the FHN model is also important to understand the dynamical properties of the model. The unknown functions play a crucial role as well as the parameters for a comprehensive approach of the model. Thus, the applications of the model with the help of numerical approaches show the results of the unknowns in a particular time interval. On the other hand, the model has been established in different types of differential equations and systems. Hence the details of the model has been considered with the different aspects. The simplified version of the model gives us understanding in the application of neural networks in biological neural concept, cardiovascular systems, deep learning and so on. The numerical investigation of such systems have been investigated by several authors including Olmos and Shizgal [2009], Chapwanya et al. [2019], Feng and Lin [2015], Fresca et al. [2020], Quarteroni et al. [2017]. The fractional FHN model has been solved numerically by an implicit numerical method with the shifted Grunwald–Letnikov approximation Liu et al. [2012], Jacobi–Gauss–Lobatto collocation method has been used for the solution of the generalized FHN equation together with time-dependent coefficients Bhrawy [2013], for solving the stochastic FHN systems some numerical and analytical methods have been improved by the authors Lindner and Schimansky-Geier [1999], Tuckwell [2008], also traveling wave solutions of FitzHugh model with cross-diffusion Berezovskaya et al. [2008] and multifront regime of a piecewise-linear FHN model with cross diffusion has been presented Zemskov et al. [2019]. Besides, bifurcation analysis of a FHN model Zhang et al. [2023], hidden extreme multistability and synchronicity of memristor-coupled non-autonomous memristive FHN models Chen et al. [2023] have been investigated. The main idea of the applications of these numerical approaches to obtain accurate results with the help of straightforward algorithmic steps based on the present model. On the other hand, numerical techniques have been implemented in various mathematical model investigations such as a trigonometric quintic B-spline method has been presented for the solution of a class of turning point singularly perturbed boundary value problems (SP-BVPs) whose solution exhibits either twin boundary layers near both endpoints of the interval under consideration or an interior layer near the turning point Alam et al. [2021]. Recently, many studies have been carried out on numerical solutions of the mathematical problems by using different methods Rahman et al. [2023], Hatipoğlu [2019], Kumar [2022], Hatipoğlu [2021]. In our research, we explore an alternative numerical approach that combines a Taylor series method with a specially constructed difference scheme. This method provides highly accurate, well established, convergent and stable results under reasonable computational conditions for solving the FHN model.

One popular relaxation oscillator for explaining how action potentials are generated in biological systems is the FHN model. Still, a thorough investigation of both analytical and numerical methods is still needed. By

re-examining the relationship between the action potential and the recovery variables through linear stability analysis, this study aims to fill this gap by providing a biological explanation to support the mathematical and numerical analyses. In particular, the work presents an alternative numerical method specifically tailored for the FHN model, which makes use of the strength of Taylor polynomials and developed difference schemes. By combining these analytical and numerical methods, the work aims to give a thorough grasp of the behaviour of the model, providing information on its stability, convergence, and robustness properties. In the numerical technique, the matrix representations, collocation points, and resulting system of nonlinear algebraic equations are presented in detail. The stability of the finite difference scheme is also investigated, which further strengthens the resilience of the numerical approach. Finally, this study aims to add to the existing body of knowledge on relaxation oscillators and action potential generation by offering a distinct and methodical analysis of the FHN model using a complementary blend of analytical and numerical methods Yönet et al. [2023], Gürbüz and Gökçe [2022], Modanlı et al. [2023].

The organisation of the paper is the following. In Section 2, the FHN model is revisited and preliminary mathematical results are presented. Here, the stability around the possible equilibria is determined via linearisation method. Eigenvalues are computed and dynamical behaviour is shown in the absence and presence of external input. Then, in Section 3, Taylor expansion to the FHN model is presented with the error estimation for the numerical solution and the convergence of the numerical technique based on Taylor truncated series are discussed. Next, in Section 4, the Difference scheme approach is constructed as an alternative route for stability analysis of the system. Finally in Section 5, summary of the results are given and potential future directions are discussed.

2 Revisiting the FHN model: preliminary mathematical results

As mentioned in Section 1, the two-variable FHN model provides a simplified but analytically-robust platform for extrapolating the central features of the HH model FitzHugh [1961], Izhikevich and FitzHugh [2006], Faghieh et al. [2010], Kostova et al. [2004]. The commonly used form of FHN model is given by

$$\begin{cases} \mu \frac{dv}{dt} = f(v, a) - \omega + I \equiv \mu F(v, \omega), \\ \frac{d\omega}{dt} = v - \gamma\omega \equiv G(v, \omega), \end{cases} \quad (1)$$

where $f(v, a) = v(a - v)(v - 1)$ with $0 < a < 1$, $\mu, \gamma > 0$.

parameter/variables	biological meaning
v	membrane potential
ω	recovery (adaptation) variable
I	input current
μ	time course for membrane potential
γ	depletion strength of recovery variable
a	threshold between electrical silence and electrical firing

Table 1: Parameters and variables used in the model (1).

Now, we briefly revisit the equilibrium, stability and bifurcation studies of the FHN model, which has been extensively studied analytically and numerically in literature.

2.1 Equilibrium and stability of the model with fixed parameters

The equilibrium point $E_* = E(v_*, \omega_*)$ of the system is found using

$$f(v_*, a) - \omega_* + I = 0 \quad \text{and} \quad v_* - \gamma\omega_* = 0, \quad (2)$$

from which

$$f(v_*, a) - \frac{v_*}{\gamma} + I = 0, \quad (3)$$

is obtained. One can draw conclusions about the stability at this point by regarding a small perturbation of the form

$$(v, \omega) = (v_*, \omega_*) + \epsilon(\psi_1(t), \psi_2(t)) + O(\epsilon^2), \quad 0 < \epsilon \ll 1. \quad (4)$$

Using a first order Taylor expansion and substituting in the model (1) the system is presented as

$$\begin{aligned} \frac{d\psi_1}{dt} &= \frac{f'(v_*, a)\psi_1(t) - \psi_2(t)}{\mu}, \\ \frac{d\psi_2}{dt} &= \psi_1(t) - \gamma\psi_2(t), \end{aligned} \quad (5)$$

where f' represents the derivative of function with respect to v . The matrix form of the system in (5) is written as

$$\frac{d}{dt} \begin{pmatrix} \psi_1 \\ \psi_2 \end{pmatrix} = \mathcal{M}|_{E_*} \begin{pmatrix} \psi_1 \\ \psi_2 \end{pmatrix}, \quad \mathcal{M}|_{E_*} = \begin{pmatrix} \frac{f'(v_*, a)}{\mu} & \frac{1}{-\gamma} \\ 1 & \mu \end{pmatrix}, \quad (6)$$

where \mathcal{M} represents the Jacobian matrix evaluated at equilibrium (v_*, ω_*) . To find non-trivial solutions, the characteristic polynomial $\text{Det}(\mathcal{M}|_{E_*} - \lambda I) = 0$ is solved for which the eigenvalues satisfy

$$2\lambda_{1,2} = -\text{Tr } \mathcal{M}|_{E_*} \pm \sqrt{\text{Tr } \mathcal{M}|_{E_*}^2 - 4 \text{Det } \mathcal{M}|_{E_*}}. \quad (7)$$

Note that, in the absence of synaptic current, i.e. $I = 0$, we have

$$f(v_*, a) - \frac{v_*}{\gamma} = -v_* \left\{ v_*^2 - (a+1)v_* + \left(a + \frac{1}{\gamma} \right) \right\} = 0, \quad (8)$$

leading to $v_*^{(1)} = 0$ and

$$v_*^{(2,3)} = \frac{(a+1)}{2} \pm \frac{\sqrt{(1-a)^2 - 4/\gamma}}{2}.$$

This implies that real $v_*^{(2)}$ and $v_*^{(3)}$ exist only if $\gamma(1-a)^2 \geq 4$. Thus a and γ parameters are indicative of the existence of non-zero membrane potential. The case $\gamma(1-a)^2 < 4$ corresponds to extinction state. The Jacobian matrix for the extinction state

$$\mathcal{M}|_{(0,0)} = \begin{pmatrix} -a & -1 \\ \mu & \mu \\ 1 & -\gamma \end{pmatrix}, \quad (9)$$

implies that $\text{Tr } \mathcal{M}|_{E_0} < 0$ and $\text{Det } \mathcal{M}|_{E_0} > 0$ for which $E_0 = (0, 0)$. Thus the extinct state is either a stable node or spiral depending on the value inside the square root in equation (7). In the case where $I \neq 0$, it is possible to have $\text{Tr } \mathcal{M} > 0$ since the equilibrium of the system introduced by equation (3) depends on the input current I . We may now look for the Hopf bifurcations that may arise when $\text{Tr } \mathcal{M} = 0$. Since the equilibrium is stable when $I = 0$, we expect an instability as I increases, followed by a restabilization for a larger value of I . It is worth to note that the existence of the equilibria $v_*^{(2,3)}$ depend on a and γ parameters and the gradient of the w -nullcline decreases as γ is increased. For $I = 0$, the nullclines intersect at only singular point (a resting state), which is a stable node. Thus, if $(1-a)^2 < 4/\gamma$ then we only have one equilibrium point at $(v_*, \omega_*) = (0, 0)$ and $f'(0) = -a$.

To validate the above analytical study, the numerical simulations of the FHN system given in (1) can be shown. Throughout the rest of the paper we keep the system parameters constant at $a = 0.22$, $\gamma = 1.18$ and $\mu = 0.008$, while varying the input current I . The initial conditions (ICs) for the system are initialised to $(v(0), \omega(0)) = (0, -0.2)$. Besides, the initial conditions (ICs) for the system are set to $(v(0), \omega(0)) = (0, -0.2)$.

Figure 1 represents recovery variable ω (a-c) and the time evolution of membrane potential v and the corresponding phase-plane diagrams (d-f) with different levels of input currents: $I = 0.05$ (a,d), $I = 0.2$ (b,e) and $I = 0.6$ (c,f). Here Fig. 1(a,d) corresponds to excitable system where the fixed point $(v_*, \omega_*) = (0.0495, 0.042)$ is a stable spiral. Figure 1(b,e) show the oscillatory behaviour of the system when input I crosses the first Hopf bifurcation. Here the equilibrium point is found to be $(v_*, \omega_*) = (0.2404, 0.2037)$ with $I = 0.2$. In addition, one can observe how with large current input the oscillations drop to the steady state $(v_*, \omega_*) = (0.8141, 0.6899)$ after passing the other bifurcation point in Fig. 1(c,f). The dashed magenta and the nullclines of the system are represented by cyan curves.

Figure 2 presents the roots of the characteristic equation, given by equation (7) for varying values of I parameter. When a small input current is incorporated in the model, two eigenvalues have negative real parts (green dots) therefore the system is a stable spiral, see Fig. 2(a). Then the first Hopf bifurcation (HB_1) occurs at a critical threshold value $I = 0.1025$, as seen in Fig. 2(a), where only a pair of imaginary ($\lambda = \pm 11.12i$) eigenvalues (magenta dots) is observed. After crossing HB_1 , e.g. for $I = 0.2$ in Figure 2(c), the positive coexisting state becomes an unstable node until it passes the second Hopf bifurcation (HB_2), that occurs at $I = 0.4963$ (not shown). Increasing the input current further, e.g. $I = 0.6$, the stability switches back from unstable to stable, where the coexisting state becomes a stable node.

2.2 Bifurcation analysis

The analytical and numerical studies presented in this section of the model have been validated by numerous works published in the literature over many years, see for example Sherwood and Model [2014], Cebrián-Lacasa et al. [2024].

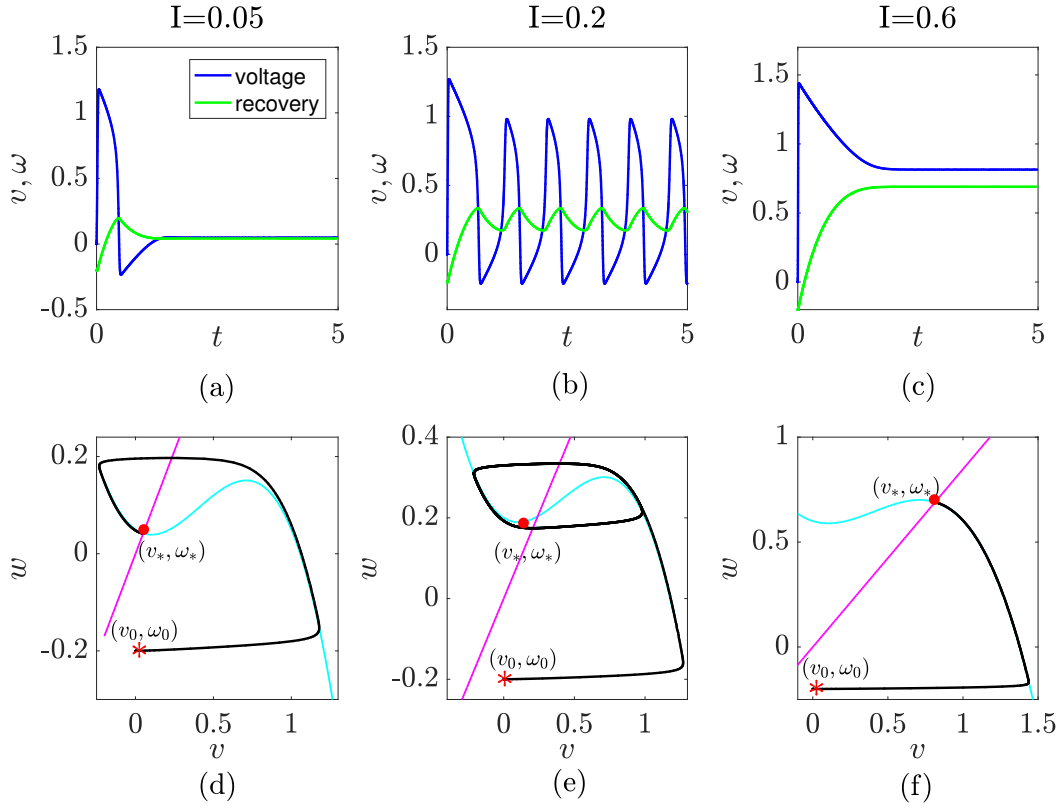


Figure 1: The trajectory of the voltage variable (blue) and recovery (green) variable are shown for different levels of input, where $I = 0.05$ (a,d), $I = 0.2$ (b,e) and $I = 0.6$ (c,f). Here (d-f) represent the corresponding phase diagrams. The red star represents the IC, that is chosen as $(v_0, \omega_0) = (0, -0.2)$. The equilibrium points for each case are shown with red dot. The dashed magenta and cyan curves represent nullclines of the system other parameters are given in the text.

For the case where $I \neq 0$, $\text{Tr} \mathcal{M}$ could be positive as the equilibrium point given by equation (3) depends on the input current. Since the equilibrium point is stable when $I = 0$, we expect an instability when input current I increases, followed by a restabilisation for larger values of I , as stated in Figs. 1 and 2.

Bifurcation diagram of the system (1) is shown in Fig. 3(a). Here the system may be considered to be excitable when the coexisting state lies on the left end of the interval for input current I (stable). On the contrary, it becomes oscillatory when the equilibrium point lies on the middle branch with dashed line (unstable). The equilibrium loses its stability through the first Hopf bifurcation (HB_1) at $\lambda_{1,2} = \pm 11.12i$, leading to a stable limit cycle surrounding unstable fixed point. Increasing the values of input current from $I = 0.1025$ to $I = 0.4963$, a small increase occurs in size of the limit cycle for higher values of input current and the system evolves to a limit cycle with a corresponding change in its size. The second Hopf bifurcation (HB_2) is encountered when input reaches to $I = 0.4963$, by which the oscillations drop to a coexisting equilibrium. Note that both bifurcations are supercritical giving rise to stable limit cycle. This can be also validated depending on the sign of the first Lyapunov coefficient Engelborghs et al. [2002]. These results are also confirmed in Fig. 3(b), where real part of the eigenvalues are plotted with respect to input parameter and stability switch is observed at two critical thresholds for Hopf points.

The bifurcation diagrams in Fig. 3 are plotted using DDE-BIFTOOL package, comprising a collection of MATLAB functions and allowing the stability analysis of fixed points and the numerical continuation of the model around the fixed points Engelborghs et al. [2002]. This package is commonly used to study continuation of the delay differential equations, yet it can also be used for systems with no delay terms. The FHN model is a mathematical model used to describe the dynamics of excitable cells, particularly neurons. The model describes the behaviour of the membrane potential (v) and a recovery variable (ω). Biologically, the FHN model captures the essential

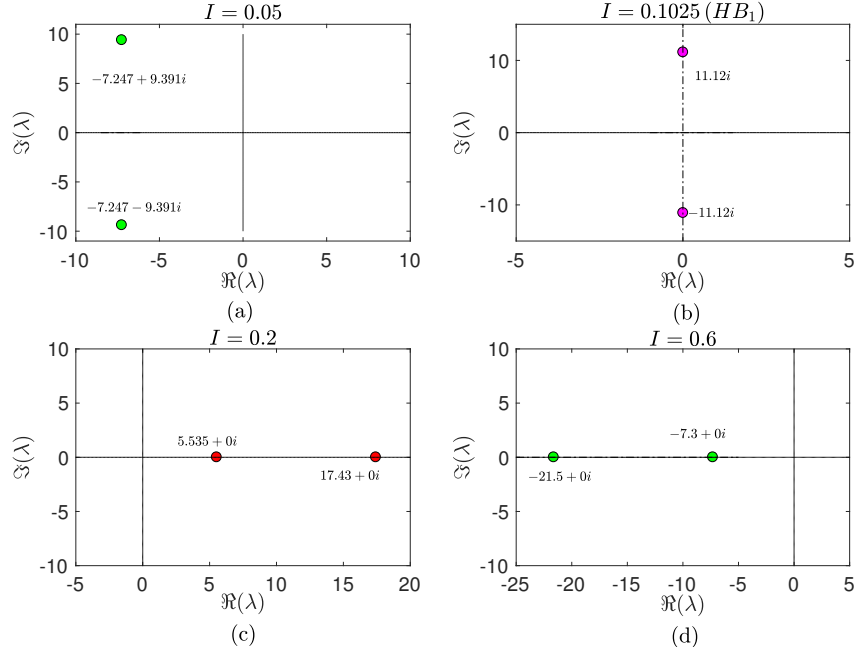


Figure 2: Spectra of steady state (v_*, ω_*) for FHN system given in (1) for different values of input I . The system is stable spiral when $I = 0.05$ (a), The first Hopf bifurcation (HB_1) occurs at $I = 0.1025$ (b), where a pair of eigenvalues with only imaginary part is obtained. The second Hopf bifurcation (HB_2) occurs at $I = 0.4963$ (not shown). The system represents an unstable node for $I = 0.2$ (c) and stable node for $I = 0.6$ (d).

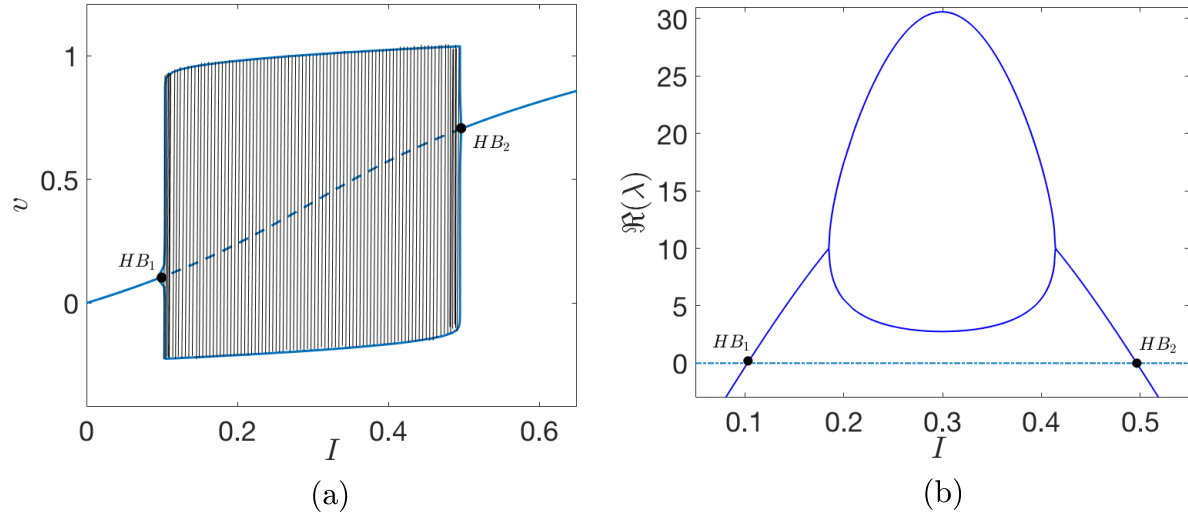


Figure 3: Bifurcation diagram of v with respect to input I (a), where solid line show stable dynamics and dashed line shows unstable dynamics with two eigenvalues with positive real parts and periodic orbits arising from HB_1 and HB_2 are observed. The real parts of the roots of the characteristic equation are plotted with respect to input I (b).

dynamics of neuronal firing. When v exceeds a certain threshold, it triggers an action potential (excitation) leading to a rapid depolarisation phase. Subsequently, ω influences the recovery phase, causing the membrane potential to return to its resting state (inhibition). Therefore, the dynamic behaviour of the model has been

obtained analytically and simulated in the figures above. This interplay between v and ω is similar to the behaviour of neurons during the firing and recovery phases of action potentials. Overall, the FHN model provides a simplified but effective representation of neuronal excitability and firing patterns that is valuable for studying the dynamics of neural networks and related phenomena.

3 Taylor Approximation to the FHN Model

In this section, we describe an algorithm for the solution of the problem defined in (1) with the ICs: $v(0) = 0$ and $\omega(0) = -0.2$. This approach gives us an alternative numerical understanding for the problem. Thus, we describe a suitable numerical algorithm for the solution of the problem. With the help of this numerical approach and its convergence, the accurate results are obtained and investigated for the infinity norm (L_∞ -Norm).

3.1 Method Description

We approximate to the system solutions in (1) by truncated Taylor series.

$$v(t) \cong v_N(t) = \sum_{n=0}^N a_{1,n}(t-c)^n \quad \text{and} \quad \omega(t) \cong \omega_N(t) = \sum_{n=0}^N a_{2,n}(t-c)^n, \quad (10)$$

where N is the Taylor polynomial degree at the point $t = c$ for $d \leq t \leq e$, for all $d, e \in \mathbb{N}$ Wang and Wang [2014]. Here we have

$$a_{1,n} = \frac{1}{n!} v^{(n)}(c) \quad \text{and} \quad a_{2,n} = \frac{1}{n!} \omega^{(n)}(c), \quad n = 1, 2, \dots, N, \quad (11)$$

the unknown coefficients $a_{1,n}$ and $a_{2,n}$ and we approximate to the numerical solution of $v(t)$ and $\omega(t)$ in the system (1) by using Taylor series approach Gürbüz and Sezer [2020], Gürbüz [2021]. Moreover we consider the collocation points defined by

$$t_i = d + \frac{e-d}{N}i, \quad i = 0, 1, \dots, N, \quad (12)$$

where we have the pointwise approximation over the interval $[d, e]$, i.e. $d = t_0 < t_1 < \dots < t_N = e$. The numerical approach is described by using the matrix relations around $c = 0$. Now we consider the matrix forms of the unknown functions, $v(t)$ and $\omega(t)$, and their derivatives Wang and Wang [2014], Gürbüz [2019]. Thus the equations in (1) are introduced in the matrix form:

$$\begin{aligned} [v'(t)] &= \mathbf{T}(t)\mathbf{B}\mathbf{A}_1 = \frac{1}{\mu}[f(v, a)] - \frac{1}{\mu}\mathbf{T}(t)\mathbf{A}_2 + \mathbf{R}, \\ [\omega'(t)] &= \mathbf{T}(t)\mathbf{B}\mathbf{A}_2 = \mathbf{T}(t)\mathbf{A}_1 - \gamma\mathbf{T}(t)\mathbf{A}_2, \end{aligned} \quad (13)$$

where \mathbf{R} is a constant matrix with respect to t . On the other hand, matrix representations of the nonlinear arguments of the system (1) are denoted by $[f(v, a)]$ which will be defined in details. Briefly,

$$[v(t)] = \mathbf{T}(t)\mathbf{A}_1 \quad \text{and} \quad [\omega(t)] = \mathbf{T}(t)\mathbf{A}_2. \quad (14)$$

Besides, we show the matrix forms of the derivatives of $v(t)$ and $\omega(t)$ in the model (1) Gürbüz and Sezer [2019], Gürbüz [2020].

$$[v'(t)] = \mathbf{T}(t)\mathbf{B}\mathbf{A}_1 \quad \text{and} \quad [\omega'(t)] = \mathbf{T}(t)\mathbf{B}\mathbf{A}_2,$$

where

$$\begin{aligned} \mathbf{T}(t) &= [1 \quad t \quad t^2 \quad \dots \quad t^N], \quad \mathbf{B} = \begin{bmatrix} 0 & 1 & 0 & \dots & 0 \\ 0 & 0 & 2 & \dots & 0 \\ \vdots & \vdots & \vdots & \ddots & \vdots \\ 0 & 0 & 0 & \dots & N \\ 0 & 0 & 0 & \dots & 0 \end{bmatrix}, \\ \mathbf{A}_1 &= [a_{10} \quad a_{11} \quad a_{12} \quad \dots \quad a_{1N}]^T, \quad \mathbf{A}_2 = [a_{20} \quad a_{21} \quad a_{22} \quad \dots \quad a_{2N}]^T. \end{aligned}$$

On the other hand, we have the function $f(v, a)$ which is defined as

$$f(v, a) = v(a-v)(v-1) = -v^3 + v^2 + v^2a - va.$$

Here the nonlinear arguments of the function $f(v, a)$ are also introduced in the matrix forms as follows Çetin et al. [2018]:

$$[f(v, a)] = -\mathbf{T}(t)\bar{\mathbf{T}}(t)\bar{\bar{\mathbf{T}}}(t)\bar{\bar{\mathbf{A}}}_1 + a\mathbf{T}(t)\bar{\mathbf{T}}(t)\bar{\mathbf{A}}_1 - a\mathbf{T}(t)\mathbf{A}_1 = \mathbf{f}(v, a),$$

where

$$[v^3] = \mathbf{T}(t)\overline{\mathbf{T}}(t)\overline{\overline{\mathbf{T}}}(t)\overline{\overline{\mathbf{A}}}_1, \quad [v^2] = \mathbf{T}(t)\overline{\mathbf{T}}(t)\overline{\mathbf{A}}_1,$$

and

$$\begin{aligned} \overline{\mathbf{T}}(t) &= \text{diag} \left(\mathbf{T}(t), \mathbf{T}(t), \dots, \mathbf{T}(t) \right), \quad \overline{\overline{\mathbf{T}}}(t) = \text{diag} \left(\overline{\mathbf{T}}(t), \overline{\mathbf{T}}(t), \dots, \overline{\mathbf{T}}(t) \right), \\ \overline{\mathbf{A}}_1 &= \begin{bmatrix} \mathbf{A}_1 & \mathbf{A}_1 & \dots & \mathbf{A}_1 \end{bmatrix}, \quad \overline{\overline{\mathbf{A}}}_1 = \begin{bmatrix} \mathbf{A}_1 a_{10} & \mathbf{A}_1 a_{11} & \dots & \mathbf{A}_1 a_{1N} \end{bmatrix}. \end{aligned}$$

Hence we have the fundamental matrix relations of the related system in (1). We use the matrix form of the system in (13) and the collocation points defined in (12) and we have

$$\begin{aligned} \mathbf{T}(t_i)\mathbf{B}\mathbf{A}_1 &= \frac{1}{\mu}f(v, a) - \frac{1}{\mu}\mathbf{T}(t_i)\mathbf{A}_2 + \mathbf{R}, \\ \mathbf{T}(t_i)\mathbf{B}\mathbf{A}_2 &= \mathbf{T}(t_i)\mathbf{A}_1 - \gamma\mathbf{T}(t_i)\mathbf{A}_2. \end{aligned} \quad (15)$$

Alternatively,

$$\begin{aligned} \left(\mathbf{T}\mathbf{B} + \frac{a}{\mu}\mathbf{T} \right) \mathbf{A}_1 - \frac{a}{\mu}\mathbf{T}\overline{\mathbf{T}}\mathbf{A}_1 + \frac{a}{\mu}\mathbf{T}\overline{\overline{\mathbf{T}}}\overline{\overline{\mathbf{A}}}_1 - \frac{1}{\mu}\mathbf{T}\mathbf{A}_2 &= \mathbf{R}, \\ -\mathbf{T}\mathbf{A}_1 + (\mathbf{T}\mathbf{B} + \gamma\mathbf{T})\mathbf{A}_2 &= \mathbf{0}. \end{aligned} \quad (16)$$

Now we write the matrix form of the ICs with the help of the relations in (14) and we have

$$[v(0)] = \mathbf{T}(0)\mathbf{A}_1 = [0], \quad \text{and} \quad [\omega(0)] = \mathbf{T}(0)\mathbf{A}_2 = [-0.2], \quad (17)$$

and it is including $[f(v(0), a)] = -\mathbf{T}(0)\overline{\mathbf{T}}(0)\overline{\overline{\mathbf{T}}}(0)\overline{\overline{\mathbf{A}}}_1 + \sigma\mathbf{T}(0)\overline{\mathbf{T}}(0)\overline{\mathbf{A}}_1 - \sigma\mathbf{T}(0)\mathbf{A}_1$ for any a . Then we replace the low matrices (17) into the alternatively written new matrix system (16) and we obtain the solutions of the fundamental matrix system in the case the determinant of the system is different than zero. Thus we get the approximate solutions in the form

$$v_N(t) = \sum_{n=0}^N \frac{1}{n!} v^{(n)}(0) t^n \quad \text{and} \quad \omega_N(t) = \sum_{n=0}^N \frac{1}{n!} \omega^{(n)}(0) t^n. \quad (18)$$

3.2 Convergence Analysis

Now we perform the error estimation for the numerical solutions of the model defined in (1). Besides, the convergence of the numerical technique based on Taylor truncated series is proved Wang and Wang [2014].

Theorem 1. Assume that the function $g(t)$ is defined on the interval $[d, e]$ for the solutions of the systems of the problem defined in (1) together with the ICs, and $u_N(t)$ is the N th order Taylor polynomial solution of $u(t)$ which is obtained from (18) for $n = 0, 1, \dots, N$. Hence

$$\|u(t) - u_N(t)\|_{\infty} \leq \frac{M}{(N+1)!} |u^{(N+1)}(\xi)| + L \max_{0 \leq n \leq N} |e_n(c)|, \quad (19)$$

where $M = \max_{d \leq t \leq e} |(t-c)^{N+1}|$, $L = \ell_{\infty}$ and $e_n(c) = u^{(n)}(c) - u_N^{(n)}(c)$ for $d \leq t \leq e$. In particular, L_{∞} -Norm is defined as $\ell_{\infty} = \max_{d \leq t \leq e} \{|l_0(c)|, |l_1(c)|, \dots, |l_n(c)|\}$.

Proof. Let us consider

$$\|u(t) - u_N(t)\|_{\infty} \leq \|u(t) - T_n(t)\|_{\infty} + \|T_n(t) - u_N(t)\|_{\infty},$$

where

$$T_n(t) = \sum_{n=0}^N \frac{u^{(n)}(c)(t-c)^n}{n!}, \quad u_N(t) = \sum_{n=0}^N \frac{u_N(c)(t-c)^n}{n!}.$$

Here we consider the residual correction together with the remainder of Taylor polynomial Wang and Wang [2014], Oliveira [1980].

$$R_n(t) = u(t) - T_n(t) = \frac{u^{(N+1)}(\xi)}{(N+1)!} (t-c)^{N+1}.$$

Thus we have

$$|R_n(t)| \leq \frac{u^{(N+1)}(\xi)}{(N+1)!} \cdot \max_{d \leq t \leq e} |(t-c)^{N+1}| = \frac{M}{(N+1)!} u^{(N+1)}(\xi). \quad (20)$$

On the other hand, we have the error function $e_n(c)$ around $t = c$ and the Taylor functions $l_n(c)$ for $n = 0, 1, \dots, N$, respectively:

$$e_n(c) = u^{(n)}(c) - u_N^{(n)}(c) \quad \text{and} \quad l_n(c) = \frac{(t-c)^n}{n!}.$$

Then we set

$$\delta_n = (e_0(c), e_1(c), \dots, e_n(c), \dots, e_N(c)), \quad \ell = (l_0(c), l_1(c), \dots, l_n(c), \dots, e_N(c))^T.$$

Hence we obtain

$$|T_n(t) - u_N(t)| = \left| \sum_{n=0}^N \left(u^{(n)}(c) - u_N^{(n)}(c) \right) \frac{(t-c)^n}{n!} \right| = |\delta_n \cdot \ell| = \|\delta_n\|_\infty \cdot \|\ell\|_\infty \leq L \|\delta_n\|_\infty. \quad (21)$$

From (20) and (21), we have

$$\begin{aligned} \|u(t) - u_N(t)\|_\infty &\leq \frac{u^{(N+1)}(\xi)}{(N+1)!} \cdot \max_{d \leq t \leq e} |(t-c)^{N+1}| + \|\ell\|_\infty \cdot \|\delta_n\|_\infty \\ &= \frac{M}{(N+1)!} |u^{(N+1)}(\xi)| + L \max_{0 \leq n \leq N} |e_n(c)|. \end{aligned}$$

This completes the proof. \square

Now we have the following Corollary results from (1):

Corollary 2. *If $g(t)$ and $u(t)$ run with Taylor polynomial functions, we obtain the Taylor polynomials solutions of (1) together with ICs. Hence we call $u_N(t)$ as the N th order Taylor polynomial solution of $u(t)$ for any $N > 0$ Wang and Wang [2014].*

Corollary 3. *If $g(t)$ and $u(t)$ are n th order differentiable functions, then $u_N(t) = T_n(t)$. Namely, we call $u_N(t)$ as the N th order Taylor polynomial solution of $u(t)$. Besides, $u_N(t)$ is described as the N th order Taylor interpolating polynomial Wang and Wang [2014].*

Hence, we complete the convergence proof of the numerical method. It is designed based on the approximation to the problem. The analysis of the method introduces therefore a suitable approximation to the problem which is defined for the FHN model. This alternative approach gives a better understanding for the appropriate results which is a novel application for such dynamic model.

4 Constructed Difference Scheme and its Stability for the FHN Model

In this section, we describe an alternative for a numerical scheme and its stability for the solution of the FHN model with the ICs given above. The numerical scheme is based on the finite difference approach. Thus, in this numerical approach we have beneficial outcome for the investigation of the model. The numerical scheme has several steps and we now explain it with its stability. We aim to find approximation to the model and understand it comprehensively. Thus, we introduce an alternative numerical scheme with the stability analysis. The discretisation of problem (1) is carried out in one step, we define the grid space Ashyralyev et al. [2021]. Now, introduce grids with uniform steps are given as

$$\overline{W^\tau} = \{t_k : t_k = k\tau, k = 0, 1, \dots, N, N\tau = T\}, \quad W^\tau = \overline{W^\tau} \cap W^\tau$$

and introduce the Hilbert space $H = L_{2\tau} = L_2(\overline{W^\tau})$ of the grid functions $\varphi^\tau(t) = \{\varphi(\tau_1 i_1, \tau_2 i_2, \dots, \tau_k i_k)\}$ defined on $\overline{W^\tau}$ equipped with the norm $\|\varphi\|$, Ashyralyev and Modanlı [2015]

$$\|\varphi^\tau\|_{2\tau} = \left(\sum_{t \in W^\tau} |\varphi^\tau| \tau_1 \tau_2 \dots \tau_k \right)^{\frac{1}{2}}. \quad (22)$$

Using Taylor expansion for the formula as to t of $v(t)$ and $\omega(t)$, the forward difference formula is obtained as

$$\begin{cases} v_t(t_k) \approx \frac{v_{k+1} - v_k}{\tau}, \\ \omega_t(t_k) \approx \frac{\omega_{k+1} - \omega_k}{\tau}. \end{cases} \quad (23)$$

The ICs can be written as $v_0 = 0, \omega_0 = -0.2$ for the system (1). The formula (23) is written into the formula (1), we have

$$\begin{cases} \omega_{k+1} = (1 - \gamma\tau)\omega_k + \tau v_k, \\ v_{k+1} = v_k + \frac{\tau}{\mu} [v_k(a - v_k)(v_k - 1) - \omega_k + I] \\ v_0 = 0, \omega_0 = -0.2. \end{cases} \quad (24)$$

Now, we will prove the theorem of stability estimates for the difference scheme formula (24).

Theorem 4. *The following stability estimates is satisfies for the formula (24) with depend on ICs as:*

$$(i) \quad \|v_k\|_H \leq \frac{\tau}{\mu} \left[\sum_{j=1}^k (\|f_{j-1} - \omega_{j-1}\|_H) + k \|I\|_H \right]$$

$$(ii) \quad \|\omega_k\|_H \leq \tau \sum_{j=1}^{k-1} \|v_j\|_H,$$

Proof. (i) From the formula (24), we can write

$$v_{k+1} = v_k + \frac{\tau}{\mu} [f_k - \omega_k + I],$$

and form that

$$v_k = v_{k-1} + \frac{\tau}{\mu} [f_{k-1} - \omega_{k-1} + I], \quad (25)$$

here $f_k = v_k(v_k - a)(v_k - 1)$. The formula (25) is clearly written as

$$\begin{aligned} v_1 &= v_0 + \frac{\tau}{\mu} [f_0 - \omega_0 + I], \quad v_0 = 0; \\ v_2 &= \frac{\tau}{\mu} [f_0 - \omega_0 + I] + \frac{\tau}{\mu} [f_1 - \omega_1 + I], \\ &\dots \\ v_k &= \frac{\tau}{\mu} [f_0 + f_1 + \dots + f_{k-1} - (\omega_0 + \omega_1 + \dots + \omega_{k-1}) + I + I + \dots + I], \\ v_k &= \frac{\tau}{\mu} \left[\sum_{j=1}^k (f_{j-1} - \omega_{j-1}) + kI \right]. \end{aligned} \quad (26)$$

Using triangle inequality and applying the norm (22) to the formula (26), we can obtain

$$\|v_k\|_H \leq \frac{\tau}{\mu} \left[\sum_{j=1}^k (\|f_{j-1} - \omega_{j-1}\|_H) + k \|I\|_H \right]. \quad (27)$$

From the extreme points of a function, it can be easily seen that the maximum point of f_k is $\frac{2}{3}$ and the minimum point of ω_k is $-\frac{1}{5}$. We know from the first and second values that f_k and ω_k functions are increasing functions. Thus, we have

$$\max_{1 \leq j \leq k} \|f_{j-1} - \omega_{j-1}\|_H = \frac{2}{3} + \frac{1}{5} = \frac{13}{15}. \quad (28)$$

Considering that $1 < k < N$, $\tau = \frac{1}{N}$ and μ is finite value, we obtain

$$\|v_k\|_H \leq \left(\frac{13\tau}{15\mu} + k \|I\|_H \right). \quad (29)$$

From (29), the stability estimates are satisfied for (29).

(ii) For the proof of the theorem, the formula (23) can be rewritten as

$$\omega_0 = -\frac{1}{5}, \quad (30)$$

$$\omega_1 = -\frac{1}{5}(1 - \gamma\tau), \quad (31)$$

$$\omega_2 = -\frac{1}{5}(1 - \gamma\tau)^2 + v_1, \quad (32)$$

$$\omega_3 = -\frac{1}{5}(1 - \gamma\tau)^3 + \tau(1 - \gamma\tau)v_1 + \tau v_2, \quad (33)$$

$$\omega_k = -\frac{1}{5}(1 - \gamma\tau)^k + \tau(1 - \gamma\tau)^{k-2}v_1 + \tau(1 - \gamma\tau)^{k-3}v_2 + \dots + v_{k-1}\tau. \quad (34)$$

Using triangle inequality and applying the norm (22) to the formula (30), we can obtain

$$\begin{aligned} \|\omega_k\|_H &= \left| -\frac{1}{5}(1 - \gamma\tau)^k \right| + |\tau(1 - \gamma\tau)^{k-2}| \|v_1\|_H + \dots \\ &\quad + |\tau(1 - \gamma\tau)^{k-3}| \|v_2\|_H + \dots + \tau \|v_{k-1}\|_H \\ &\leq 1 + \tau[\|v_1\|_H + \|v_2\|_H + \dots + \|v_{k-1}\|_H] \\ &\leq \tau \sum_{j=1}^{k-1} \|v_j\|_H. \end{aligned} \quad (35)$$

Using the formula (29), the stability estimates are satisfied for the formula (35). Thus, we complete the proof of the theorem. \square

Let us now present the numerical results of the problem defined in (1) together with the ICs. By using the formula (24) and MATLAB programming, we have the simulations which are shown in Figures (4) and (5), respectively.

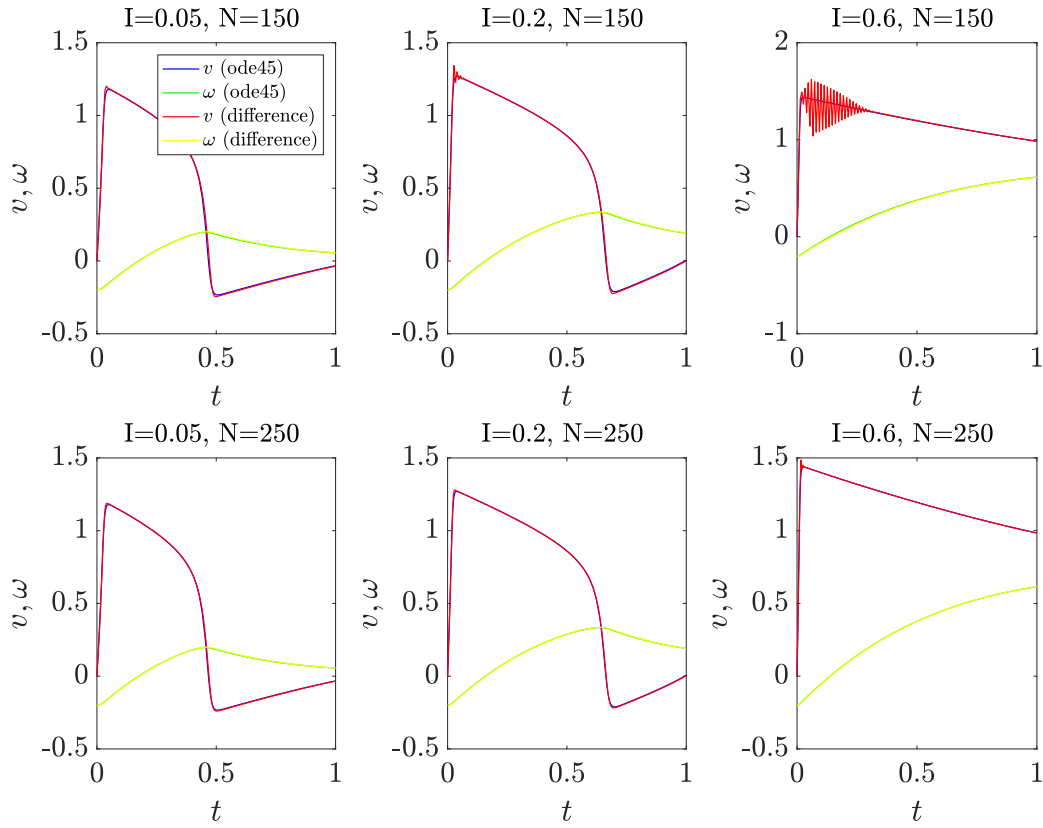


Figure 4: Gives the approximation solutions of $v(t)$ and $\omega(t)$ for $\mu = 0.008$, $\gamma = 1.18$, $a = 0.22$, and $0 \leq t \leq 1$.

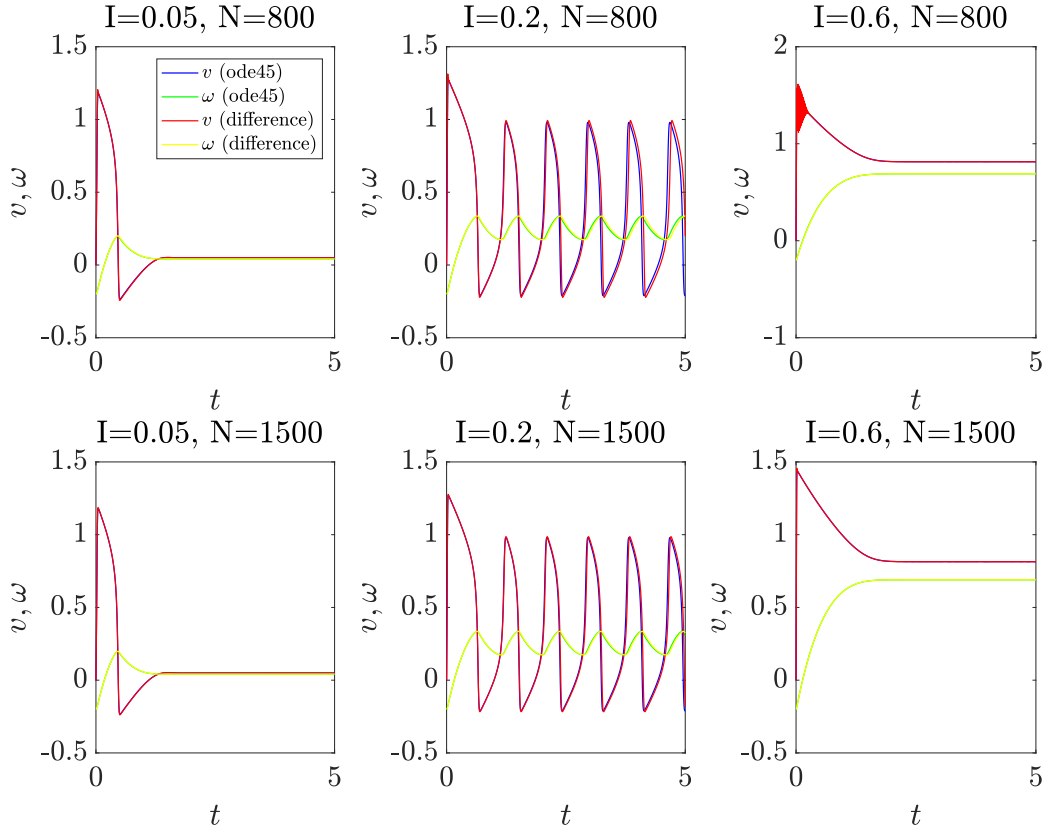


Figure 5: Gives the approximation solutions of $v(t)$ and $\omega(t)$ for $\mu = 0.008$, $\gamma = 1.18$, $a = 0.22$, and $0 \leq t \leq 5$.

From Figures 4 and 5, $\omega(t)$ increases up to given value in the formula (29), while $v(t)$ decreases up to that value. After this value, it continues in parallel as depending on the formula (35). However, as the number of N intervals increases, the physical appearance of the figures becomes clearer as the ω and v functions are closer to their real values. At the same time, as the t time interval widens, the behavior of the figures becomes more pronounced, for example from 4 to 5.

We now investigate the convergency rates of the numerical approach in (3) for the L_∞ -Norm Feng and Lin [2015], Heydari et al. [2012]. This gives us a better understanding for the Taylor approach together with the Finite Difference approximation results. Here we also consider the parameters as follows: $I = 0.6$, $\mu = 0.008$, $\gamma = 1.18$, $a = 0.22$, and $\tau = 0.00025$, for $0 \leq t \leq 1$. From Table (2) and Table (3), we can easily see that the numerical approach ensures efficient results for higher order N values. Thus the numerical approach has beneficial findings whenever we reach for larger iterations. We can also understand that the approximations for the different truncation limits have analogue results at the L_∞ -Norm.

t	$N = 4$	$N = 5$	$N = 6$
0.0	0.10620E-3	0.11630E-4	0.13978E-5
0.1	0.11560E-3	0.15122E-4	0.13596E-5
0.2	0.13323E-3	0.18851E-4	0.13671E-5
0.3	0.10003E-3	0.14520E-4	0.14582E-5
0.4	0.11588E-3	0.15505E-4	0.14896E-5
0.5	0.13994E-3	0.11091E-4	0.19071E-5
0.6	0.14278E-3	0.19985E-4	0.13601E-5
0.7	0.13775E-3	0.20120E-4	0.14772E-5
0.8	0.15953E-3	0.20512E-4	0.14850E-5
0.9	0.15029E-3	0.20001E-4	0.12417E-5
1.0	0.19003E-3	0.35277E-4	0.11230E-4

Table 2: Error convergence of approximated $v(t)$ for the L_∞ -Norm and $N = 4, 5$ and 6 , respectively.

Besides Figure 6 shows us that the behaviour of the convergency results shows similarities even for the different unknowns in the system, $v(t)$ and $\omega(t)$. On the other hand, these L_∞ -Norm of error functions show that the behaviour of these functions vary for the same interval where we have $[0, 1]$.

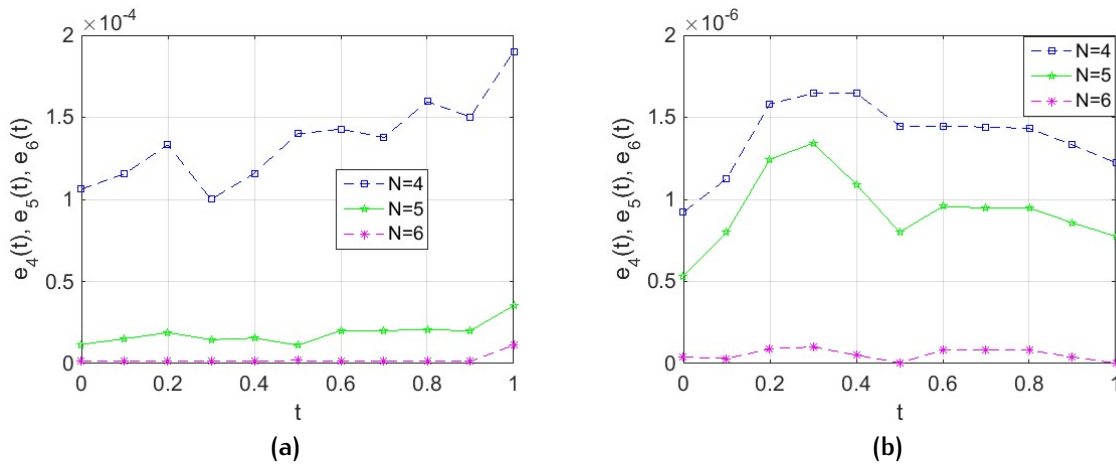


Figure 6: The L_∞ -Norm of error functions for $N = 4, 5$ and 6 , respectively, where (a) shows the results for $v(t)$ and (b) $\omega(t)$.

In particular, the L_∞ -Norm of error function of $v(t)$ has complication which has been also basically seen in Figure 6. Namely, the unknown function has the L_∞ -Norm of its error function has increasing outcome which is visible in Figure 6 and at Table 2. There is also seen that $\omega(t)$ has been simply exponentially growing function. Thus the L_∞ -Norm of error function of $\omega(t)$ has decreasing error results which is seen in Figure 6 and at Table 3. The computation time for various numerical schemes has been analysed for N and simulation time t Olmos and Shizgal [2009]. The calculation per unit (CPU) (s) is obtained for the comparison values for the speed of t . As an example, for the fixed parameters, ICs and $N = 4, 5$ and 6 for $\omega(t)$ at $0 \leq t \leq 1$, we obtain the CPU (s): 0.111 s, 0.175s, and 0.188s, respectively.

t	$N = 4$	$N = 5$	$N = 6$
0.0	0.09217E-5	0.05309E-5	0.04012E-6
0.1	0.11259E-5	0.08000E-5	0.03015E-6
0.2	0.15822E-5	0.12443E-5	0.08928E-6
0.3	0.16448E-5	0.13418E-5	0.10092E-6
0.4	0.16449E-5	0.10919E-5	0.05097E-6
0.5	0.14476E-5	0.80021E-6	0.04902E-7
0.6	0.14445E-5	0.95708E-6	0.81000E-7
0.7	0.14409E-5	0.94712E-6	0.85011E-7
0.8	0.14319E-5	0.94810E-6	0.80031E-7
0.9	0.13318E-5	0.85701E-6	0.40122E-7
1.0	0.12231E-5	0.77500E-6	0.01884E-7

Table 3: Error convergence of approximated $\omega(t)$ for the L_∞ -Norm and $N = 4, 5$ and 6 , respectively.

5 Conclusion

The study purposes a comprehensive analysis of the FHN model problem defined in (1) with ICs. Firstly, the model is revisited with its equilibrium and stability analysis via a characteristic polynomial. In fact, the linearisation of this nonlinear system near the equilibrium points is key to determine the stability with the eigenvalues found by the Jacobian matrix. Depending on the value of the external input current (I), stable and unstable dynamics through a limit cycle around the positive equilibrium are shown as an example. The model results have been studied and confirmed by the authors, see for example Izhikevich and FitzHugh [2006], Faghhi et al. [2010], Kostova et al. [2004].

The highlight of this manuscript is to introduce a numerical method based on the truncated Taylor series and provide alternative approaches to obtain the solutions and stability of the system. In this regard, Taylor polynomial approach has been applied on the model problem and we have the convergency result of the method. Moreover, finite difference scheme has been performed and numerical simulations of the results have been obtained. Thus, the FHN model is motivated by the numerical approaches which show us appropriate dynamical results of the unknown functions in the model. The straightforwardness of the combined technical application gives a novelty for the scientific computing approach. Namely, we have completed a comprehensive numerical application with a highly motivated FHN model described in details with its stability analysis and the bifurcation approach. This consequence is supported by the figures and the tables where we can easily see the beneficial outcome. The results can be also enriched by the different values of the parameters and adapted for the different systems. The numerical scheme based on Taylor polynomials is of advantageous outcomes regarding the convergency results and the explicit procedure in the concept of an algorithmic approach Gürbüz et al. [2021]. Although this paper presents a thorough investigation of the FHN model using analytical and numerical techniques, certain limitations should be noted. To account for complicated dynamics, approximations are used in the linear stability analysis and local stability conditions. Precision and computational resource limitations affect the numerical simulations. Although developed for this model, the innovative Taylor polynomial and built difference scheme approaches have not been as effective or scalable to larger frameworks. The FHN model is also a simplistic representation that may not fully capture all biological nuances. Despite these drawbacks, the work provides a useful framework for studying relaxation oscillators and opens the door for further studies that address these limitations, consider different models and improve numerical techniques. On the other hand, finite difference scheme for the problem concluded the approximation with highly reasonable results which is uniquely designed as an alternative approach for the problem. The combination of the numerical schemes for the FHN model open new tasks for the future investigation and introduce a novel approximation for the which will be essential for the further research on approximation for such dynamical system problems.

Furthermore, the model can be dealt with its different aspects. In particular, the numerical scheme applied here can be considered for the stochastic analysis of the FHN model as a future Outlook. Besides, the simplification of the FHN model can be obtained by using a piecewise-linear transformation. Thus we can get mathematically more attainable McKean model and we compare the results from the theoretical and numerical aspects McKean Jr [1970]. Following the ideas presented in Gökçe [2021], Gürbüz and Rendall [2022], the extension of the study is also possible with a spatial diffusion term which is to describe the voltage variable and we compare the dynamics in terms of various theoretical and numerical schemes of partial differential equations and travelling wave analysis by including the time delay. In addition, by adapting the model and using data-driven methods, such as any deep learning approach, it can also be applied to in-depth investigations that are in high demand Zeng et al. [2022], Kossaczka et al. [2023].

References

- R. FitzHugh. Impulses and physiological states in theoretical models of nerve membrane. *Biophys. J.*, 1(6):445, 1961.
- J. Nagumo, S. Arimoto, and S. Yoshizawa. An active pulse transmission line simulating nerve axon. *Proc. IRE*, 50(10):2061–2070, 1962.
- C. Rocsoreanu, A. Georgescu, and N. Giurgiteanu. *The FitzHugh–Nagumo model: bifurcation and dynamics*, volume 10. Springer Science & Business Media, 2012.
- H.C. Tuckwell and R. Rodriguez. Analytical and simulation results for stochastic FitzHugh–Nagumo neurons and neural networks. *J. Comput. Neurosci.*, 5(1):91–113, 1998.
- C.K.R.T. Jones. Stability of the travelling wave solution of the FitzHugh–Nagumo system. *Trans. Am. Math. Soc.*, 286(2):431–469, 1984.
- S. Sato and S. Doi. Response characteristics of the BVP neuron model to periodic pulse inputs. *Math. Biosci.*, 112(2):243–259, 1992.
- E.M. Izhikevich and R. FitzHugh. FitzHugh–Nagumo model. *Scholarpedia*, 1(9):1349, 2006.
- W.E. Sherwood, D. Jaeger, and R. Jung. Fitzhugh–nagumo model., 2014.
- R.T. Faghih, K. Savla, M.A. Dahleh, and E.N. Brown. The FitzHugh–Nagumo model: Firing modes with time-varying parameters & parameter estimation. In *2010 Annual International Conference of the IEEE Engineering in Medicine and Biology*, pages 4116–4119. IEEE, 2010.
- T. Kostova, R. Ravindran, and M. Schonbek. FitzHugh–Nagumo revisited: Types of bifurcations, periodical forcing and stability regions by a lyapunov functional. *Int. J. Bifurcation Chaos*, 14(03):913–925, 2004.
- O. O. Onyejekwe. Dynamical computations of the FitzHugh–Nagumo equation. *Archive J. Biomed. Sci. Eng.*, 7(1):027–036, 2021.
- E.M. Izhikevich, N. S. Desai, E.C. Walcott, and F.C. Hoppensteadt. Bursts as a unit of neural information: selective communication via resonance. *Trends Neurosci.*, 26(3):161–167, 2003.
- A.M. Pertsov, E.A. Ermakova, and A.V. Panfilov. Rotating spiral waves in a modified FitzHugh–Nagumo model. *Physica D*, 14(1):117–124, 1984.
- B.N. Vasiev, P. Hogeweg, and A.V. Panfilov. Simulation of Dictyostelium discoideum aggregation via reaction–diffusion model. *Phys. Rev. Lett.*, 73(23):3173, 1994.
- R.R. Aliev and A.V. Panfilov. A simple two–variable model of cardiac excitation. *Chaos, Solitons Fractals*, 7(3):293–301, 1996.
- L. Glass and M.E. Josephson. Resetting and annihilation of reentrant abnormally rapid heartbeat. *Phys. Rev. Lett.*, 75(10):2059, 1995.
- A. Panfilov and J.P. Keener. Re–entry in an anatomical model of the heart. *Chaos, Solitons Fractals*, 5(3–4):681–689, 1995.
- J.D. Murray. *Mathematical biology II: spatial models and biomedical applications*, volume 3. Springer New York, 2001.
- X. Liao, L.Q. Wang, and P. Yu. *Stability of dynamical systems*. Elsevier, 2007.
- R. Seydel. *Practical bifurcation and stability analysis*, volume 5. Springer Science & Business Media, 2009.
- D. Olmos and B. D. Shizgal. Pseudospectral method of solution of the fitzhugh–nagumo equation. *Math. Comput. Simulat.*, 79(7):2258–2278, 2009.
- M. Chapwanya, O. A. Jejenywa, A. R. Appadu, and J. S. Lubuma. An explicit nonstandard finite difference scheme for the FitzHugh–Nagumo equations. *Int. J. Comput. Math.*, 96(10):1993–2009, 2019.
- H. Feng and R. Lin. A finite difference method for the FitzHugh–Nagumo equations. *Dyn. Contin. Discrete Impuls. Syst. B: Appl. Algorithms*, 22:401–412, 2015.
- S. Fresca, A. Manzoni, L. Dedè, and A. Quarteroni. Deep learning–based reduced order models in cardiac electrophysiology. *Dyn. Contin. Discrete Impuls. Syst. B: Appl. Algorithms*, 15(10):e0239416, 2020.
- A. Quarteroni, A. Manzoni, and C. Vergara. The cardiovascular system: mathematical modelling, numerical algorithms and clinical applications. *Acta Numer.*, 26:365–590, 2017.
- F. Liu, I. Turner, V. Anh, Q. Yang, and K. Burrage. A numerical method for the fractional FitzHugh–Nagumo monodomain models. *Anziam J.*, 54:608–629, 2012.

- A. H. Bhrawy. A Jacobi–Gauss–Lobatto collocation method for solving generalized FitzHugh–Nagumo equation with time-dependent coefficients. *Appl. Math. Comput.*, 222:255–264, 2013.
- B. Lindner and L. Schimansky-Geier. Analytical approach to the stochastic FitzHugh–Nagumo system and coherence resonance. *Phys. Rev. E*, 60(6):7270, 1999.
- H. C. Tuckwell. Analytical and simulation results for the stochastic spatial FitzHugh–Nagumo model neuron. *Neural Comput.*, 20(12):3003–3033, 2008.
- F. Berezovskaya, Wirkus S. Camacho, E., and G. Karev. Traveling wave solutions of fitzhugh model with cross-diffusion. *Math. Biosci. Eng.*, 5(2):239–260, 2008.
- E. P. Zemskov, M. A. Tsyganov, and W. Horsthemke. Multifront regime of a piecewise-linear fitzhugh-nagumo model with cross diffusion. *Phys. Rev. E*, 99(6):062214, 2019.
- X. Zhang, Dou Y. Min, F., and Y. Xu. Bifurcation analysis of a modified fitzhugh-nagumo neuron with electric field. *Chaos Soliton. Frac.*, 170:113415, 2023.
- M. Chen, X. Luo, Y. Suo, Q. Xu, and H. Wu. Hidden extreme multistability and synchronicity of memristor-coupled non-autonomous memristive fitzhugh-nagumo models. *Nonlinear Dyn.*, 111(8):7773–7778, 2023.
- M. P. Alam, D. Kumar, and A. Khan. Trigonometric quintic b-spline collocation method for singularly perturbed turning point boundary value problems. *Int. J. Comput. Math.*, 98(5):1029–1048, 2021.
- M. E. Rahman, A. Kumar, and S. Singh. On the nonlinear characteristics of two-phase flow system as modified fitzhugh-nagumo model. *Int. J. Heat Mass Transf.*, 207:123963, 2023.
- V. F. Hatipoğlu. A numerical algorithm for the solution of nonlinear fractional differential equations via beta-derivatives. *Math. Method. Appl. Sci.*, 42(16):5258–5265, 2019.
- D. Kumar. A uniformly convergent scheme for two-parameter problems having layer behaviour. *Int. J. Comput. Math.*, 99(3):553–574, 2022.
- V. F. Hatipoğlu. A novel model for the contamination of a system of three artificial lakes. *Discrete Contin. Dyn. Syst. - S*, 14(7):2261–2272, 2021.
- N. Yönet, B. Gürbüz, and A. Gökçe. An alternative numerical approach for an improved ecological model of interconnected lakes with a fixed pollutant. *Comput. Appl. Math.*, 42(1):56, 2023.
- B. Gürbüz and A. Gökçe. An algorithm and stability approach for the acute inflammatory response dynamic model. In *Operations Research*, pages 192–217, 2022.
- M. Modanlı, M. A. S. Murad, and S. T. Abdulazeez. A new computational method-based integral transform for solving time-fractional equation arises in electromagnetic waves. *Z. Angew. Math. Phys.*, 74(5):186, 2023.
- William Erik Sherwood and FitzHugh–Nagumo Model. *Encyclopedia of computational neuroscience*, 2014.
- Daniel Cebrián-Lacasa, Pedro Parra-Rivas, Daniel Ruiz-Reynés, and Lendert Gelens. Six decades of the fitzhugh-nagumo model: A guide through its spatio-temporal dynamics and influence across disciplines. *Physics Reports*, 1096:1–39, 2024.
- K. Engelborghs, T. Luzyanina, and D. Roose. Numerical bifurcation analysis of delay differential equations using dde-biftool. *ACM Trans. Math. Softw.*, 28(1):1–21, 2002.
- K. Wang and Q. Wang. Taylor collocation method and convergence analysis for the Volterra–Fredholm integral equations. *J. Comput. Appl. Math.*, 260:294–300, 2014.
- B. Gürbüz and M. Sezer. Modified operational matrix method for second-order nonlinear ordinary differential equations with quadratic and cubic terms. *Int. J. Optim. Control: Theor. Appl.*, 180(2):218–225, 2020.
- B. Gürbüz. A computational approximation for the solution of retarded functional differential equations and their applications to science and engineering. *J. Ind. Manage. Optim.*, 2021.
- B. Gürbüz. Laguerre matrix-collocation technique to solve systems of functional differential equations with variable delays. *AIP Conf. Proc.*, 2183(1):090007, 2019.
- B. Gürbüz and M. Sezer. Laguerre matrix-collocation method to solve systems of pantograph type delay differential equations. In *Proceedings of the International Conference on Computational Mathematics and Engineering Sciences*, pages 121–132. Springer, Cham., 2019.
- B. Gürbüz. A numerical investigation on a neural field model. In *Proceedings of the 4th International Conference on Mathematics: "An Istanbul Meeting for World Mathematicians"*, pages 685–695, 2020.
- M. Çetin, B. Gürbüz, and M. Sezer. Lucas collocation method for system of high-order linear functional differential equations. *J. Arts Sci. Tech.*, 180(4):891–910, 2018.

- F. A. Oliveira. Collocation and residual correction. *Numer. Math.*, 36(1):27–31, 1980.
- A. Ashyralyev, D. Ağırseven, and K. Türk. On the stability of second order of accuracy difference scheme for the numerical solution of the time delay telegraph equation. *AIP Conf. Proc.*, 2325(1):020032, 2021.
- A. Ashyralyev and M. Modanlı. An operator method for telegraph partial differential and difference equations. *Boundary Value Probl.*, 2015(1):1–17, 2015.
- H. Heydari, Z. Avazzadeh, and G. B. Loghmani. Chebyshev cardinal functions for solving Volterra–Fredholm integrodifferential equations using operational matrices. *Iran. J. Sci. Technol.*, 36(1):13–24, 2012.
- B. Gürbüz, H. Mawengkang, I. Husein, and G.W. Weber. Rumour propagation: an operational research approach by computational and information theory. *Cent. Eur. J. Oper. Res.*, pages 1–21, 2021.
- H.P. McKean Jr. Nagumo’s equation. *Adv. Math.*, 4(3):209–223, 1970.
- A. Gökçe. A mathematical study for chaotic dynamics of dissolved oxygen–phytoplankton interactions under environmental driving factors and time lag. *Chaos, Solitons Fractals*, 151:111268, 2021.
- B. Gürbüz and A.D. Rendall. Analysis of a model of the Calvin cycle with diffusion of ATP. *Discrete Contin. Dyn. Syst. - B*, 2022.
- K. Zeng, A. J. Linot, and M. D. Graham. Data-driven control of spatiotemporal chaos with reduced-order neural ode-based models and reinforcement learning. *Proc. R. Soc. (London) A*, 478(2267):20220297, 2022.
- T. Kossaczká, M. Ehrhardt, and M. Günther. Deep fdm: Enhanced finite difference methods by deep learning. *J. Frank. Inst.*, 4:100039, 2023.